IEEE Access
Multidisciplinary | Rapid Review | Open Access Journal

Received 14 October 2023, accepted 5 December 2023, date of publication 7 December 2023,
date of current version 18 December 2023.

Digital Object Identifier 10.1109/ACCESS.2023.3340414

RESEARCH ARTICLE

Modeling and Lyapunov-Based Nonlinear Control Strategies of Novel 2-D Inverted Magnetic Needle System: A Comparative Study

P. SURESH KUMAR[1], B. ASHOK[2], HOSSAM KOTB[3], KAREEM M. ABORAS[3], AND SEADA HUSSEN[4]

[1]Automotive Research Centre, Vellore Institute of Technology, Vellore, Tamil Nadu 632014, India
[2]School of Mechanical Engineering, Vellore Institute of Technology, Vellore, Tamil Nadu 632014, India
[3]Department of Electrical Power and Machines, Faculty of Engineering, Alexandria University, Alexandria 21544, Egypt
[4]Department of Electrical Power, Adama Science and Technology University, Adama 1888, Ethiopia

Corresponding author: Seada Hussen (seada.hussen@aastu.edu.et)

ABSTRACT This research investigates control theory using an advanced two-dimensional inverted magnetic needle system. The complex dynamics of the system are caused by a non-uniform external magnetic field. The system dynamics are established using Euler's equations, and an energy-based controller is proposed to stabilize the needle near an unstable equilibrium point. We propose energy-based control techniques and compare their performance to the Model Predictive Controller (MPC) performance. An important contribution of this research is the rigorous investigation of closed-loop system stability using Lyapunov function analysis and tracking the performance of energy-based control techniques and MPC controller. The dynamic behavior of the magnetic needle is further enriched by two rotational degrees of freedom, influenced by attractive and repulsive forces from external magnets. Moreover, we assess the effectiveness of energy-based control strategies in both uniform and non-uniform magnetic fields, thereby expanding the applications of control theory.

INDEX TERMS Control theory, industrial applications, energy-based controller, 2-D inverted magnetic needle system, non-uniform magnetic field, system stability, tracking performance.

I. INTRODUCTION

Over the last five decades, researchers have extensively used the inverted pendulum system as a standard for control system studies. Its basic mechanical structure and nonlinear dynamics have fueled advancements in nonlinear control theory and resulted in advances in tackling practical problems. This system has a wide range of applications in aerospace engineering, such as launch vehicles and missiles, as well as robotics, such as Segway and Pendubot [1], [2], [3], [4], [5]. The inverted pendulum problem's complexity is valuable for real-world applications where gravitational potential energy plays a significant role. Its applications have proven crucial for stabilizing systems affected by external forces, demonstrating the practical translation of research and development efforts. Overall, the inverted pendulum system is an indispensable tool for control system researchers.

When considering the use of the inverted pendulum as a benchmark problem, the Earth's uniform magnetic field limits its applicability in control theory. However, for studying interstellar travel and spacecraft experiencing varying gravity fields from stars and planets, the inverted magnetic needle system has been proposed as an alternative. This system relies on a magnetic needle's potential energy, which is directly influenced by the non-uniform external magnetic fields commonly encountered. While this study assumes a constant external magnetic field, similar to the one generated by permanent magnets, incorporating a time-varying external magnetic field using electromagnets significantly increases the model's complexity.

The associate editor coordinating the review of this manuscript and approving it for publication was Dong Shen.

To accurately model real-world conditions, introducing a time-varying external magnetic field is essential. However, this complexity presents research opportunities. The goal of this paper is to achieve two objectives: accurately model the dynamics of the magnetic needle system, consider uniform and non-uniform external magnetic fields, and design energy-based control strategies for stability and optimal performance using Lyapunov's function. Simulations compare the performance and stability of these control strategies and propose energy-efficient optimal control strategies to achieve the desired reference position with minimal energy. Modeling an inverted magnetic needle system with a time-varying magnetic field and further exploration are beyond the scope of this paper.

The 2-D magnetic needle system provides two degrees of rotational flexibility in the needle. Because of the attractive and repulsive forces between the external magnets and the magnetic needle, this system has both stable and unstable equilibrium positions. When the opposite poles of external magnets and the magnetic needle are aligned, the magnetic needle will be in a stable equilibrium state. In the opposite case, if the poles are not aligned, the magnetic needle will be in an unstable equilibrium state. The external magnetic flux density and the magnetic needle dipole moment influence the torque on the magnetic needle. The external magnetic field pattern can be altered by varying the distance between the permanent magnets. Modeling a non-uniform external magnetic field increases the complexity of the dynamics involved. Analyzing such complex system dynamics may lead to the development of rich, nonlinear control methods. This paper presents a novel 2-D magnetic needle system with important implications for developing new control techniques and validating existing ones. Although the system bears some similarities to a pendulum system, the 2-D magnetic needle system has more complex dynamics, given its nonlinear external magnetic field.

A. LITERATURE REVIEW

The inverted pendulum system is a benchmark problem in control theory, with strong nonlinear dynamics and under-actuation. In this paper, we do not consider under actuation for the magnetic needle system which is left for future work. The most famous types of inverted pendulum systems are, Furuta Pendulum [6], [7], mobile inverted pendulum [8], [9], cart pendulum [10], cart-pendulum with limited track [11], the double inverted pendulum on a cart [12], [13], triple inverted pendulum [14], spherical pendulum [15], mobile inverted pendulum [16]. The stability of the inverted pendulum structure during earthquakes is studied in [17]. Nonlinear system modeling and controller design and its stability analysis are discussed in [18] and [19]. The stabilization of the inverted pendulum using a model predictive and optimal fuzzy controller is given in [20], [21], [22], and [23]. Experimental validation of pendulum stabilization using sliding mode controller is discussed in [24], [25], [26], and [27]. Validation of state feedback and conventional controller [28] and the advantages of the fuzzy controller over energy-based controller performance in stabilizing inverted pendulum, underactuated systems is explained in [29] and [30]. In [31], [32], and [33], the design of a passivity-based controller (PBC) for the electromechanical system is discussed.

The study on the energy-based controller design for stabilizing and improving the performance of an inverted pendulum system was given in [34] and [35]. Further, the robust performance of robust adaptive super-twisting sliding mode controller, back-stepping sliding mode control, and cascaded fractional order controller performance of inverted pendulum system was discussed in [36], [37], and [38]. The magnetic needle in an inverted position is restricted to one degree of freedom in [39] and [40]. The dynamics of the magnetic needle system were modeled under a uniform magnetic field [41]. In this paper, we introduce a unique and novel two-dimensional inverted magnetic needle system that has not been previously explored. The nonlinear dynamics of the system are derived using the Euler-Lagrange equation. By providing a detailed analysis of the energy-based controller design for the two-dimensional inverted magnetic needle system dynamics, this paper makes a significant contribution to the field of control engineering. A comprehensive analysis of the closed-loop system stability is provided, and the tracking performance of various control strategies is assessed through comparative simulations. This investigation is conducted by taking into account both uniform time-invariant external magnetic fields and non-uniform external magnetic fields. The contributions of the paper are given below,

- Establishing of two-dimensional inverted magnetic needle system dynamics through Euler's equations considering a non-uniform magnetic field.
- External magnetic flux density 3D modeling using the Gaussian function with minimum modeling error.
- Design of energy-based control strategies to stabilize the needle near an unstable equilibrium point.
- Comparing energy-based control strategies with Model Predictive Controller (MPC).
- Closed-loop system stability using a Lyapunov function analysis.

B. MOTIVATION

Inverted pendulum systems are useful for theoretical and practical purposes. Theoretical research on these systems sheds light on key topics such as stability, controllability, and robustness. In practice, they serve as a standard in control engineering, allowing for the evaluation and optimization of control algorithms for a variety of real-world problems. In robotics, inverted pendulum systems help to develop stability-enhancing control strategies, which enhance activities like balancing and humanoid robots in areas like uneven terrain navigation, agile movement execution, and overall control improvement. These systems are also important in increasing the safety, maneuverability, and user experience of self-balancing vehicles such as Segways and electric

scooters. Additionally, they aid in designing algorithms that reduce unwanted movements in camera gimbals, resulting in stabilized footage, or control strategies that minimize vibrations in industrial machinery to enhance stability.

II. INTRODUCTION TO NOVEL 2-D INVERTED MAGNETIC NEEDLE SYSTEM

The 2-D inverted magnetic needle system enables the needle to have two degrees of freedom as depicted in Fig. 1. In this setup, two external magnets with opposite poles facing one another are placed, and the distance between them is adjustable, providing a means to introduce significant non-linearity in the external magnetic field if needed. The magnetic needle experiences torque, which depends on the distance from the external magnets. To allow free rotation about the pivot point, the magnetic needle is pivoted at its center using motor M_2 with one degree of freedom. Furthermore, the shaft of motor M_1 is rigidly attached to the center of motor M_2.

The system inertial coordinates denoted as X_i, Y_i, and Z_i are considered, while the needle body coordinates are represented by x_b, y_b, and z_b. The external magnets are arranged such that the direction of the magnetic field lies along the negative X_i-axis. Motor M_1 rotation occurs about the Z_i-axis, and the right-hand coordinate system is completed by the Y_i-axis. The magnetic needle body coordinates are defined as follows: the magnetic needle length is oriented along the x_b-axis, and the rotation of motor M_2 is defined as the y_b-axis, while the z_b-axis conforms to the right-hand rule of the coordinate system.

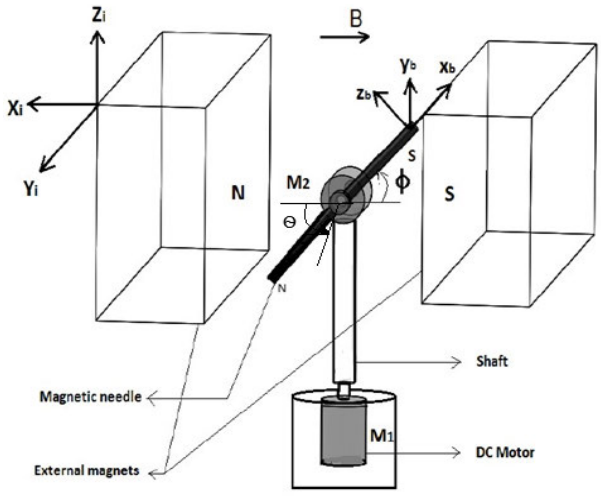

FIGURE 1. Schematic of 2-D magnetic needle system.

III. MODELING SYSTEM DYNAMICS THROUGH EULER'S EQUATIONS

A. SYSTEM MODELING WITH UNIFORM MAGNETIC FIELD

The system dynamics are derived using Euler equations,

$$\frac{d}{dt}\left(\frac{\partial T}{\partial \dot{\phi}}\right)-\frac{\partial T}{\partial \phi}+\frac{\partial U}{\partial \phi}=\tau_{y_m},\ \frac{d}{dt}\left(\frac{\partial T}{\partial \dot{\theta}}\right)-\frac{\partial T}{\partial \theta}+\frac{\partial U}{\partial \theta}=\tau_{z_m} \tag{1}$$

where system kinetic and potential energy are represented by T & U, respectively. Fig. 2 illustrates the rotation of motor M_2 along the y_m axis, while motor M_1 rotation is represented along the z_m axis. The motor control input torque about the y_m and z_m axes is represented by τ_{y_m} and τ_{z_m}, respectively.

1) POTENTIAL ENERGY

The system potential energy depends on the external magnetic field B, and needle dipole moment M, and the system potential energy is:

$$U = MB(1+\cos\theta\cos\phi) \tag{2}$$

The system dynamics are derived in the generalized coordinates of the motor M_2, as shown in Fig. 2. The rotation angle about z_m axis is considered as θ, and the rotation angle about the y_m axis is defined as ϕ.

A permanent magnet's magnetic dipole moment indicates both the direction and intensity of the magnet's magnetic field. The steps below are used to compute it: The magnet should first be placed in a known field in order to measure the force or torque it experiences in order to estimate the strength of the magnetic field. Next, determine the magnet's length, width, and thickness by measuring its physical dimensions. Determine the magnet's volume using these measurements. To find the magnetic moment, multiply the strength of the magnetic field by the volume of the magnet. Lastly, use the well-known right-hand rule to find the magnetic moment's direction. This rule states that the magnetic moment's direction is perpendicular to both the direction of the magnetic field and the direction of the force or torque experienced.

2) KINETIC ENERGY

The system's kinetic energy is determined by several factors, including the angular velocity and inertia of the magnetic needle. Specifically, the angular velocity about the y_m and z_m-axes is denoted by $\dot{\phi}$ and $\dot{\theta}$, respectively. Notably, the magnetic needle is free to rotate about both the y_m and z_m-axes, which are mutually perpendicular. By taking into account the individual kinetic energy about each axis, the system's total kinetic energy can be expressed as the sum of these values.

$$T = \frac{I_{y_m}\dot{\phi}^2}{2}+\frac{I_{z_m}\dot{\theta}^2}{2} \tag{3}$$

System generalized coordinates are chosen to be (x_m, y_m, z_m), at the center of mass C_g as shown in Fig. 2.

System inertia in y_m-axis,

$$I_{y_m} = \frac{m_n(3r_n^2+l_n^2)}{12} \tag{4}$$

System inertia about z_m-axis is,

$$\begin{aligned} I_{z_m} &= I_S + I_{M_2} + I_{M_1R} + I_{M_1G} + I_N \\ &= \frac{m_s r_s^2}{2} + \left(\frac{m_{M_2}(3r_{M2}^2+l_{M2}^2)}{12} + m_{M_2}x^2\right) + I_{M_1R} \end{aligned}$$

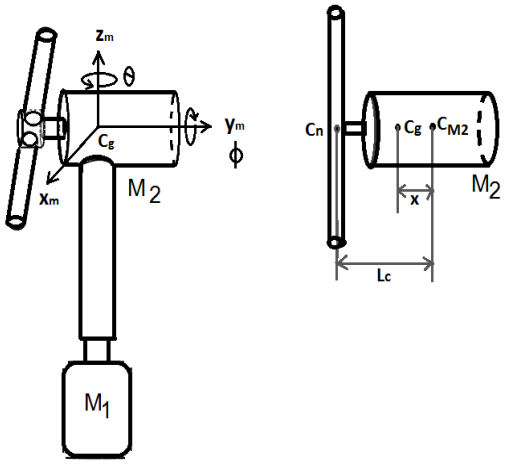

FIGURE 2. Proposed setup.

$$+ I_{M_1G} + \left(\sin^2(\phi) I^{xx} + \cos^2(\phi) I^{zz} + m_n(L_c - x)^2\right) \tag{5}$$

where, I_S is the shaft inertia which is joining the motor M_1 and M_2, I_{M_2} is the motor M_2 inertia about z_m-axis. The rotor and gearbox inertia of the motor M_1 is represented by I_{M_1R} & I_{M_1G}, and the needle inertia about z_m-axis is represented by I_N, and $I^{x_bx_b}$, $I^{z_bz_b}$ represents the needle inertia about its principal axis of x_b and z_b. The system center of mass is found using (6), where, C_n is the needle center of mass and motor M_2 center of mass is represented by C_{M_2}. The distance between the C_{M_2} and system common center of mass C_g is x, and C_n, C_{M_2} is L_c.

$$m_n(L_c - x) = m_{M_2} x \tag{6}$$

The system dynamics is derived from (2), (3), and (1).

$$\ddot{\phi} = \frac{1}{I_{y_m}} \left(\tau_{y_m} - 9.74 * 10^{-5} \sin(2\phi)\dot{\theta}^2 + MB\cos\theta\sin\phi\right) \tag{7}$$

$$\ddot{\theta} = \frac{1}{I_{z_m}} \left(\tau_{z_m} + 1.94 * 10^{-4} \sin(2\phi)\dot{\phi}\dot{\theta} + MB\cos\phi\sin\theta\right) \tag{8}$$

The 2-D inverted magnetic needle system exhibits two equilibria, located at $(\phi, \dot{\phi}, \theta, \dot{\theta})$. At $(\pi, 0, 0, 0)$, the magnetic needle is in a state of stable equilibrium, as evidenced by the negative eigenvalues. Conversely, the system is found to be unstable at (0, 0, 0, 0), since it features a positive eigenvalue.

B. SYSTEM MODELING WITH NON-UNIFORM MAGNETIC FIELD

To derive the system dynamics of a given system using Euler equations, it is necessary to have a clear understanding of its kinetic and potential energies. In the preceding section, we obtained these values for the system under consideration by assuming a uniform magnetic field. In this section, we will instead consider a non-uniform magnetic field and re-derive the system dynamics accordingly. Although the system's kinetic energy remains the same for both uniform and non-uniform magnetic fields, the potential energy for the non-uniform external magnetic field (NUEMF) case is discussed next.

C. POTENTIAL ENERGY

In an inverted pendulum system, the potential energy of the pendulum depends on its height and acceleration due to gravity.

$$U_p = mgh$$

The potential energy of a pendulum is described by U_p, with m representing the mass of the pendulum, g representing the acceleration due to gravity, and h representing the height of the pendulum relative to some reference level. In an inverted pendulum system, the pendulum's height is a function of its angle concerning the vertical, and as this angle changes, so too does the pendulum's height. As a result of this observation, we can conclude that the potential energy of the pendulum varies as a function of both its height and angle, due to the constant value of acceleration caused by gravity.

The system potential energy U_n depends on the magnetic needle torque as,

$$U_n = -\int_0^{\phi}\int_0^{\theta} (\tau) d\theta d\phi \tag{9}$$

where, magnetic needle torque τ depend on dipole moment $\mathbf{M}$, external magnetic field $\mathbf{B}$ as,

$$\tau = M \times B$$

The magnetic needle dipole moment is

$$M = \begin{bmatrix} M\sin\phi\cos\theta & M\sin\phi\sin\theta & M\cos\phi \end{bmatrix} \tag{10}$$

The external magnetic flux density is,

$$B = \begin{bmatrix} Bx & By & Bz \end{bmatrix}$$

D. MODELING OF NON-UNIFORM EXTERNAL MAGNETIC FIELD

The dipole approximation of a rectangular-cross-section bar permanent magnets is discussed in [42]. The magnetic field of the external magnets is found using COMSOL, and it is compared with the dipole approximation. The non-uniform external magnetic field modeling using COMSOL software has < 2 % error. External magnetic field x, y, and z components are modeled using the Gaussian function, and the parameters of this Gaussian function are chosen to get an optimal fit for B_x, B_y, and B_z. In Fig. 3, the relation between the standard deviation and modeling error is shown.

The external magnetic field x-component B_x variations are shown in Fig.4. It is minimum, when ϕ equals to $\pi/2$ rad and θ equals to $\pi/3$, $4\pi/3$ rad. Similarly, it is maximum, when ϕ equals to $\pi/2$ rad and θ equals to $2\pi/3$, $5\pi/3$ rad.

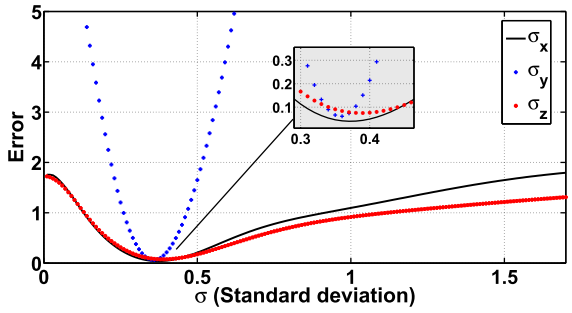

FIGURE 3. Standard deviation for best approximation of B_x, B_y, B_z.

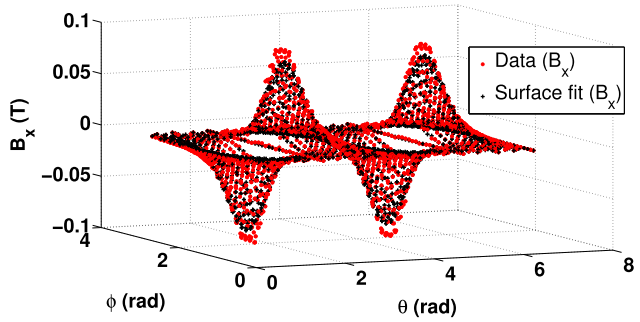

FIGURE 4. Surface fitting using Gaussian function for B_x component.

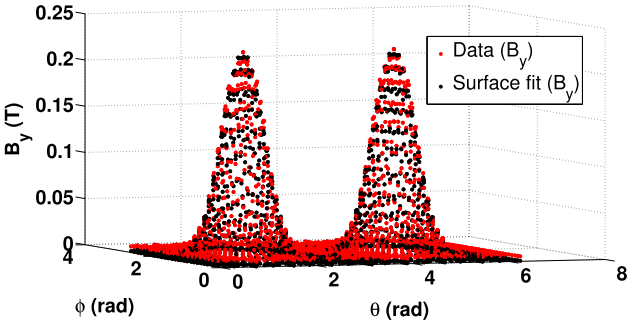

FIGURE 5. Surface fitting using Gaussian function for B_y component.

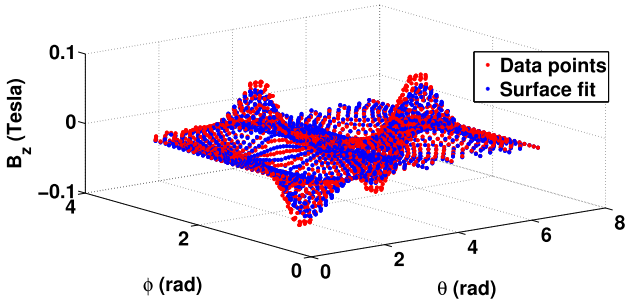

FIGURE 6. Surface fitting using Gaussian function for B_z component.

The x-component of the external magnetic field variations with respect to θ, ϕ is modeled using the Gaussian function, with a standard deviation of $\sigma_x = 0.37$ as,

$$B_x = -0.09\left(e^{-(a(\theta-1.2)^2+c(\phi-\pi/2)^2)}+e^{-(a(\theta-4.3)^2+c(\phi-\pi/2)^2)}\right) + 0.09\left(e^{-(a(\theta-1.9)^2+c(\phi-\pi/2)^2)}+e^{-(a(\theta-5.1)^2+c(\phi-\pi/2)^2)}\right) \tag{11}$$

where,

$$a = \frac{1}{2\sigma_x^2}, \quad b = 0, \quad c = \frac{1}{2\sigma_x^2}$$

Figure 5 illustrates variations in the y-component of an external magnetic field as a function of θ and ϕ. More specifically, the maximum flux density near the poles of the external permanent magnets leads to a maximum at both the stable and unstable equilibrium points. The system itself exhibits a stable equilibrium at $(\pi/2, \pi/2)$ rad, and an unstable equilibrium at $(3\pi/2, \pi/2)$ rad.

The external magnetic field y-component is modeled using the Gaussian function, with a standard deviation of $\sigma_y = 0.36$,

$$B_y = 0.2\left(e^{-(a(\theta-\pi/2)^2+c(\phi-\pi/2)^2)} + e^{-(a(\theta-4.7)^2+c(\phi-\pi/2)^2)}\right) \tag{12}$$

In Fig.6 the external magnetic field z-component variations are shown, and it is modeled using Gaussian function with a standard deviation of $\sigma_z = 0.39$,

$$B_z = -0.094\left(e^{-(a(\theta-\pi/2)^2+c(\phi-1.7)^2)} + e^{-(a(\theta-4.7)^2+c(\phi-1.9)^2)}\right) + 0.093\left(e^{-(a(\theta-\pi/2)^2+c(\phi-1.9)^2)} + 0.093e^{-(a(\theta-4.7)^2+c(\phi-1.17)^2)}\right) \tag{13}$$

In Fig. 7, the torque τ_z acting on the magnetic needle about Z-axis due to the external magnetic field x, and y-components are shown.

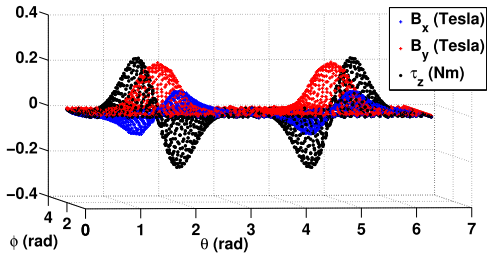

FIGURE 7. Torque about Z-axis.

The magnetic needle initially aligns with the X-axis while the external magnetic field is aligned with the Y-axis, based on the chosen coordinate system. As θ increases, the external magnet's south pole attracts the north pole of the needle, resulting in a torque in the positive Z-axis. When θ exceeds $\pi/2$ radians, the attraction between the needle and external magnet causes the torque to shift towards the negative Z-axis. At π radians, a repulsive force occurs between the north poles of the needle and external magnet, leading to a torque in the negative Z-axis. Figure 7 shows that as θ increases to $3\pi/2$ radians, the torque returns to the positive Z-axis because of

the repulsive force between the needle and the north pole of the external magnet.

System kinetic energy about Y, Z-axes,

$$T_y = \frac{I_{y_m}\dot{\phi}^2}{2}, \quad T_z = \frac{I_{z_m}\dot{\theta}^2}{2} \tag{14}$$

System dynamics is derived from (9), (14),

$$\ddot{\phi} = \frac{1}{I_{y_m}}\left(\tau_{y_m} - \frac{\partial U_n}{\partial \phi}\right), \ddot{\theta} = \frac{1}{I_{z_m}}\left(\tau_{z_m} - \frac{\partial U_n}{\partial \theta}\right)$$

IV. LYAPUNOV-BASED OPTIMAL NONLINEAR CONTROL STRATEGIES FOR OPTIMAL PERFORMANCE AND CLOSED-LOOP SYSTEM STABILITY

In robotics and control theory, an energy-based controller is a kind of controller that makes use of the idea of energy shaping to produce better control outcomes. This type of control has gained popularity recently because it makes complicated systems controllable without necessitating a thorough understanding of the dynamics at play. The energy of the system is described as a function of its state variables by the energy function. In order to maintain stable functioning, the controller's main goal is to direct the system's energy to a specified equilibrium or limit cycle. Traditional control techniques, on the other hand, usually focus on directly manipulating the positions or velocities of the system, which can be far more challenging and inefficient.

Compared to conventional control methods, the energy-based control strategy offers a number of benefits. First, the controller can guarantee stability under a variety of initial conditions since it employs a state-independent energy function. Second, the controller is structure-preserving, meaning that it maintains any inherent structural properties of the system under control, such as symmetry and conservation laws. Finally, the approach often simplifies the design process and reduces controller complexity, leading to lower implementation costs. Energy-based control techniques have been widely used in various domains, such as power systems, robotics, aerospace, and mechanical systems, and have shown significant improvements in terms of system stability, robustness, and energy efficiency.

A. NONLINEAR OPTIMAL CONTROL STRATEGIES FOR UNIFORM MAGNETIC FIELD SYSTEM

Energy is the basic property of the general physical systems (electrical, mechanical). The supplied energy E_S to the passive system is equal to the sum of stored E_{st} and dissipated energy E_d i.e,

$$E_S = E_{st} + E_d$$

System stability can be analyzed based on the system input and output energy. Nonlinear and time-varying systems can be controlled by controlling the energy of the system. The controller is designed to shape the energy storage function of the system, to have minimum energy at the desired point.

The magnetic needle has minimum energy at a stable position and maximum energy at an unstable position. Initially, a magnetic needle is positioned at an unstable equilibrium, and different control strategies are designed to equate the system energy to the desired energy E_D. The total system energy E_T is the sum of potential energy (2) and kinetic energy (3),

$$E_T = MB(1 + \cos\theta\cos\phi) + \frac{I_{y_m}\dot{\phi}^2}{2} + \frac{I_{z_m}\dot{\theta}^2}{2} \tag{15}$$

The energy corresponding to the desired position,

$$E_D = MB(1 + \cos\theta_d\cos\phi_d) \tag{16}$$

where, θ_d and ϕ_d represents the magnetic needle desired angular position about z_m, y_m axis. Energy storage function υ is considered as [43],

$$\upsilon = (E_T - E_D)^2/2, \quad \frac{d\upsilon}{dt} = (E_T - E_D)\frac{dE_T}{dt} \tag{17}$$

The condition for closed-loop system stability is,

$$\frac{d\upsilon}{dt} \leq 0 \tag{18}$$

The controller is designed to satisfy the above condition. System total energy with respect to time,

$$\frac{dE_T}{dt} = \frac{dU}{dt} + \frac{dT}{dt}$$

Change in potential energy with respect to time is,

$$\frac{dU}{dt} = -MB(\dot{\phi}\cos\theta\sin\phi + \cos\phi\sin\theta\dot{\theta})$$

To design the controller, one should know how the acceleration affects rate of system kinetic energy, which is,

$$\frac{dT}{dt} = I_{y_m}\dot{\phi}\ddot{\phi} + I_{z_m}\dot{\theta}\ddot{\theta}$$

From (7) and (8), change in system kinetic energy concerning time is,

$$\frac{dT}{dt} = \dot{\phi}\left(\tau_{y_m} - 9.74 * 10^{-5}\sin(2\phi)\dot{\theta}^2 + MB\cos\theta\sin\phi\right) + \dot{\theta}\left(\tau_{z_m} + 1.94 * 10^{-5}\sin(2\phi)\dot{\phi}\dot{\theta} + MB\cos\phi\sin\theta\right)$$

The rate of system total energy depends on the angular velocity of the needle and the motor control input as,

$$\frac{dE_T}{dt} = \dot{\phi}\tau_{y_m} + \dot{\theta}\tau_{z_m} \tag{19}$$

Different control strategies are designed to satisfy the system's closed-loop stability condition (18). The first control strategy is,

$$\tau_{y_{m1}} = -(E_T - E_D)\dot{\phi}, \quad \tau_{z_{m1}} = -(E_T - E_D)\dot{\theta}$$

In steady-state, system output has sustained oscillations (see Fig. 8) using this control strategy. A second control strategy is designed to improve the system performance, by increasing the controller gain and by limiting the angular

velocity of the magnetic needle. The second control strategy using "sgn" is chosen as,

$$\tau_{y_{m2}} = -K_y(E_T - E_D)\text{sgn}(\dot{\phi}),\ \tau_{z_{m2}} = -K_z(E_T - E_D)\text{sgn}(\dot{\theta})$$

System steady-state performance is further improved using "sat" function in the third control strategy, by reducing the amplitude of oscillations,

$$\tau_{y_{m3}} = -K_y(E_T - E_D)\text{sat}(\dot{\phi}),\ \tau_{z_{m3}} = -K_z(E_T - E_D)\text{sat}(\dot{\theta})$$

The performance of individual control strategies is discussed in the following section in detail.

B. NONLINEAR OPTIMAL CONTROL STRATEGIES FOR NON-UNIFORM MAGNETIC FIELD SYSTEM

In a feedback control system for an inverted pendulum, the controller strives to maintain the pendulum at a vertical position by regulating the system's potential energy. By measuring and modifying the state of the system using feedback, it can make the necessary adjustments to regulate the system's potential energy, maintaining a stable, upright position for the pendulum.

In a magnetic needle system, controllers based on energy are designed to hold the needle at a desired position while also satisfying closed-loop stability conditions. The needle is allowed to rotate about two perpendicular axes. The total energy for each axis is computed as the sum of its potential and kinetic energies E_{Ty}, E_{Tz}.

$$E_{Ty} = T_y + U_y, \qquad E_{Tz} = T_z + U_z$$

where, system kinetic and potential energy about Y-axis is T_y & U_y, similarly, about Z-axis T_z & U_z. System energy storage function corresponding to Y and Z-axis is υ_y & υ_z,

$$\upsilon_y = (E_{Ty} - E_{Dy})^2/2, \quad \upsilon_z = (E_{Tz} - E_{Dz})^2/2$$

where energy corresponding to the desired position of the magnetic needle about Y and Z-axis is E_{Dy} & E_{Dz}.

The condition for closed-loop system stability is,

$$\frac{d\upsilon_y}{dt} \leq 0, \qquad \frac{d\upsilon_z}{dt} \leq 0, \tag{20}$$

We consider the first control strategy as,

$$\tau_{y_1} = -(E_{Ty} - E_{Dy})\dot{\phi},\ \tau_{z_1} = -(E_{Tz} - E_{Dz})\dot{\theta}$$

From the above-designed control strategies we can observe that, as the magnetic needle reaches the desired position, the system's total energy is almost equal to the energy corresponding to the desired position. The control input goes to zero because it depends on the difference between the system's total energy and the desired energy. In steady-state, the system output has sustained oscillations using τ_{y_1}, τ_{z_1} about y_m, z_m-axes. The steady-state performance is improved by limiting the angular velocity of the magnetic needle using "sgn" function and by increasing the controller gain. However, the system output has a small amplitude of oscillations in steady-state as shown in Fig. 13 & 14, because of using "sgn" function in the controller design. The second control strategy using "sgn" function is,

$$\tau_{y_2} = -K_y(E_{Ty} - E_{Dy})\text{sgn}(\dot{\phi}),$$
$$\tau_{z_2} = -K_z(E_{Tz} - E_{Dz})\text{sgn}(\dot{\theta})$$

When compared with the other control strategies' performance, better closed-loop system performance is achieved using "sat" function in the controller design as shown in Fig. 13 & 14. Because the control of the needle angular velocity is smooth when we use "sat" function compared to "sgn" function. Third control strategy using "sat" function is given by,

$$\tau_{y_3} = -K_y(E_{Ty} - E_{Dy})\text{sat}(\dot{\phi}),$$
$$\tau_{z_3} = -K_z(E_{Tz} - E_{Dz})\text{sat}(\dot{\theta})$$

TABLE 1. System parameters.

Motor parameters	Specifications
Motor M_1, M_2 mass (m_{M_1}, m_{M_2})	60g
Motor M_2 radius (r_{M_2})	10mm
Motor M_2 length (l_{M_2})	60mm
Motor M_1 rotor inertia ($I_{M_{1rz}}$)	$0.32 * 10^{-7} Kgm^2$
Motor M_1 gear box inertia ($I_{M_{1gz}}$)	$5.5 * 10^{-7} Kgm^2$
Terminal resistance (R_a)	0.331 Ω
Terminal inductance (L_a)	0.103 mH
Motor torque constant (K_m)	0.4368 Nm/A
Back emf constant (K_b)	0.4208 V-sec/rad

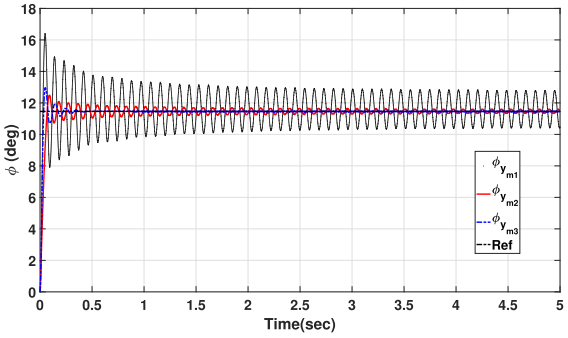

FIGURE 8. System response for different control strategies about y_m-axis.

V. SIMULATION RESULTS

A. COMPARATIVE STUDY OF ENERGY-BASED CONTROL STRATEGIES FOR UNIFORM MAGNETIC NEEDLE SYSTEM

The control strategies are designed using the Lyapunov function to improve the system output response, and to satisfy the closed-loop system stability. The actuator and sensor nonlinearities are considered to analyze the actual system behavior in simulation. System parameters are considered in Table. 1,

The system reference input (Ref) is considered to be 0.2 radians from the unstable equilibrium. System output response of different control strategies about y_m, z_m-axis are shown in Fig. 8, & 9.

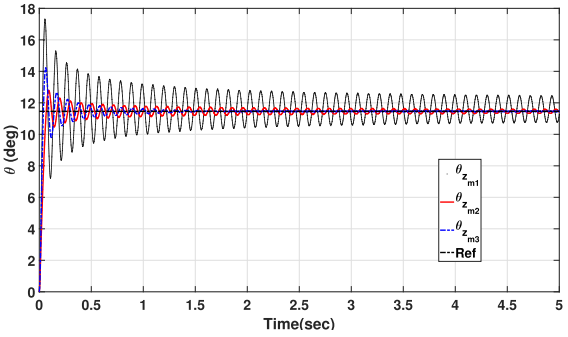

FIGURE 9. System response for different control strategies about z_m-axis.

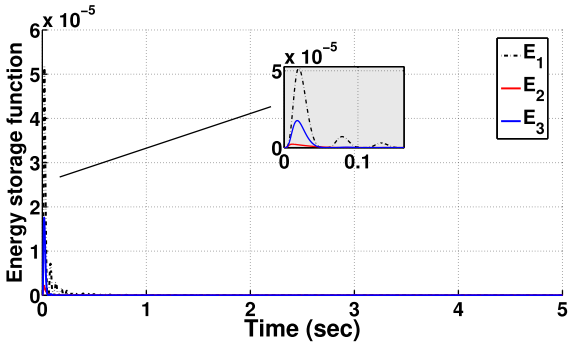

FIGURE 10. System energy storage function.

The angular position of the magnetic needle about a different axis is $\phi_{y_{m1}}$, $\phi_{y_{m2}}$ and $\phi_{y_{m3}}$, about y_m-axis for the corresponding control input voltage $V_{y_{m1}}$, $V_{y_{m2}}$, $V_{y_{m3}}$. Similarly, $\theta_{z_{m1}}$, $\theta_{z_{m2}}$ and $\theta_{z_{m3}}$ are the angular position of the magnetic needle about z_m-axis for the corresponding control voltages of $V_{z_{m1}}$, $V_{z_{m2}}$, $V_{z_{m3}}$.

In steady-state, system output has sustained oscillations from 0.18 to 0.22 radians, when we use the first control strategy $\tau_{y_{m1}}$. The system output performance is improved by increasing the controller gain and by limiting the angular velocity of the magnetic needle using "sgn" function in the second control strategy $\tau_{y_{m2}}$. The steady-state performance is further improved by using "sat" function in the third control strategy $\tau_{y_{m3}}$.

The relation between the acceleration of the magnetic needle and control input τ_{y_m} & τ_{z_m} is given in (7) & (8). Different control strategies are designed by considering torque, as a control input. To know whether the control input is physically realizable or not, torque is converted into voltage using the motor dynamics (21). The relation between the applied input voltage V, back emf voltage V_b and voltage drop across the armature resistance R and inductance L [44] is,

$$\tau_m = K_m i, \qquad V = iR + L\frac{di}{dt} + V_b \tag{21}$$

The relation between the energy storage function, E_T, and E_D is given in (17). In Fig. 10, system energy storage function (υ) variations with respect to time for the different control strategies is shown. As the magnetic needle reaches the desired position, total system energy is almost equal to the energy corresponding to the desired position. So, the difference between the system's total energy and the desired energy is almost zero at the steady state. Here E_1, E_2 and E_3 represents the system energy storage function for different control strategies.

B. SYSTEM PERFORMANCE COMPARISON WITH MPC CONTROLLER AND DIFFERENT CONTROL STRATEGIES OF ENERGY-BASED CONTROLLER

The MPC controller is an advanced control technique widely used in various industries and applications. It operates as a feedback control mechanism, utilizing a mathematical model of the system, constraints, and optimization objectives. This allows it to calculate optimal control actions at each time step. The controller's performance parameters, such as robustness and aggressiveness, can be adjusted by modifying parameters like prediction horizon (Np), control horizon (Nc), input constraints, weights, and sampling time. Fig. 11, and 12, shows the effectiveness of the MPC controller and energy-based control techniques in closed-loop systems. As shown in the figure, the MPC controller performs better than energy-based control approaches in both transient and steady-state situations.

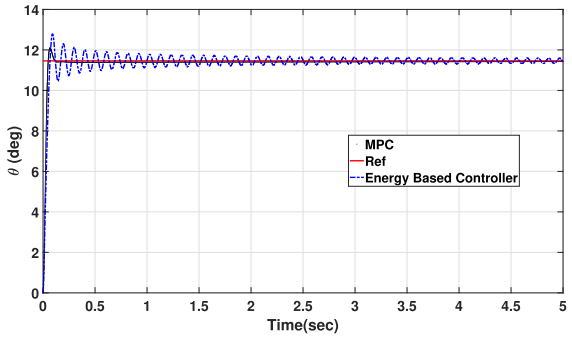

FIGURE 11. System performance comparison with MPC controller and $\tau_{y_{m3}}$.

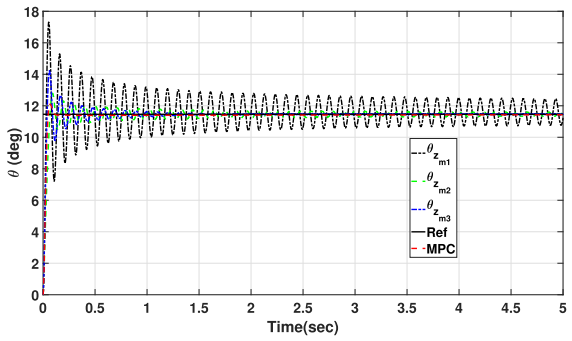

FIGURE 12. System performance comparison with MPC controller and Energy-based control strategies.

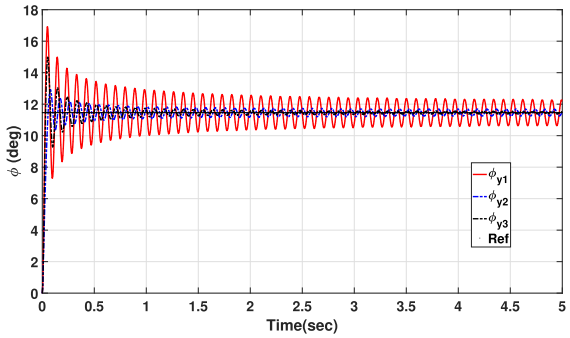

FIGURE 13. System response for different control strategies about y_m-axis.

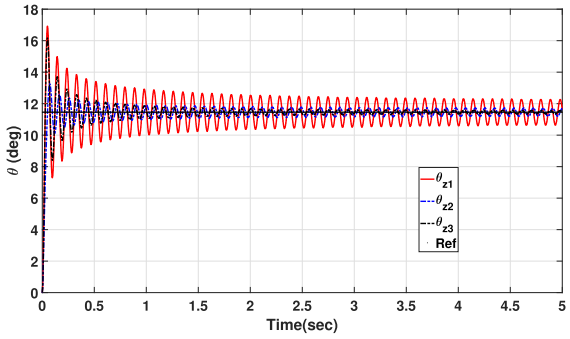

FIGURE 14. System response for different control strategies about z_m-axis.

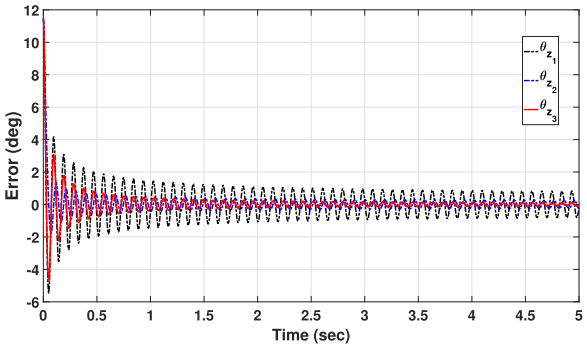

FIGURE 15. Tracking error of different control strategies about z_m-axis.

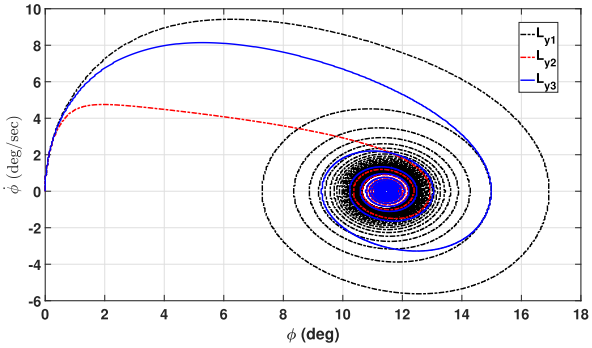

FIGURE 16. Limit cycle behavior of different control strategies about y_m-axis.

C. COMPARATIVE STUDY OF ENERGY-BASED CONTROL STRATEGIES FOR NON-UNIFORM MAGNETIC NEEDLE SYSTEM

The tracking and steady-state performance of different control strategies are discussed in this section. These control strategies are derived to hold the magnetic needle at its desired position. Tracking the performance of different control strategies about the Y-axis is shown in Fig. 13. System output has more amplitude of oscillations in steady-state, using τ_{y1}. The steady-state response is improved using the "sgn" function and by increasing the controller gain in τ_{y2}. Further, the tracking and steady-state performance are improved by using the "sat" function in τ_{y3}. Similarly, different control strategies are designed to improve the system output response about the Z-axis. The system output response of different control strategies about the Z-axis is shown in Fig. 14.

A limit cycle is a stable periodic motion in which the system's state variables fluctuate about a set point or trajectory for a specified time before returning to that point or trajectory. Limit cycle behavior refers to the stable periodic motion of the system's energy state in the context of an energy-based controller. In general, energy-based controllers strive to reduce the energy of the system under control. Long-lasting oscillations may arise when the controller is unable to bring the system to the intended state.

An energy-based control system maintains stable operation by controlling the system's energy to a predetermined equilibrium or limit cycle. When the controller's actions cause the system's energy to attain a stable periodic state, the result is the limit cycle behavior. This form of oscillatory behavior, which has a fixed amplitude and frequency, is commonly seen in simple nonlinear systems like oscillators.

Control systems can gain from limit cycle behavior in a number of ways, including increased energy efficiency and system stability. But it can also result in unfavorable outcomes like noise or wear and tear. As a result, understanding and controlling limit cycle behavior is essential when designing control systems. The tracking error of various control strategies is illustrated in Fig. 15. The first control strategy exhibits limit cycle behavior with a ± 1 degrees tracking error amplitude. The second strategy reduces the tracking error to ± 0.25 degrees. However, the third control strategy outperforms the others, limiting the tracking error to ± 0.1 degrees.

Limit cycle behavior is observed in the system output using different control strategies about y_m and z_m-axis, which shows the relation between the angular position and angular velocity. The angular velocity varies from 10 to -5 rad/sec using the first control strategy, and the system output has a sustained oscillation in the steady state about y_m and z_m-axes. This steady state performance is improved by limiting the angular velocity using a "sat" function as shown in Fig. 16 & 17.

In the context of the system's control strategies, Fig. 18 provides insights into the variation of the energy storage

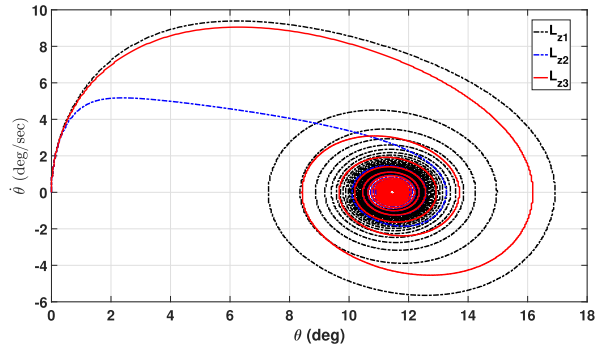

FIGURE 17. Limit cycle behavior of different control strategies about z_m-axis.

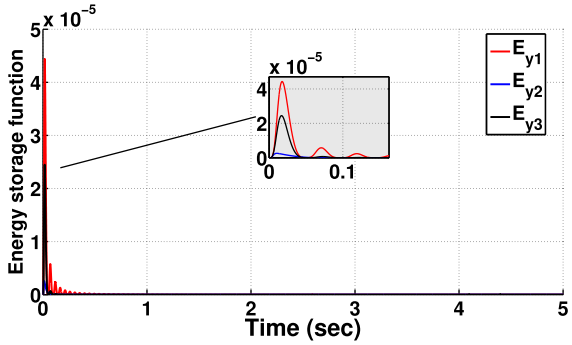

FIGURE 18. Energy storage function about y_m-axis.

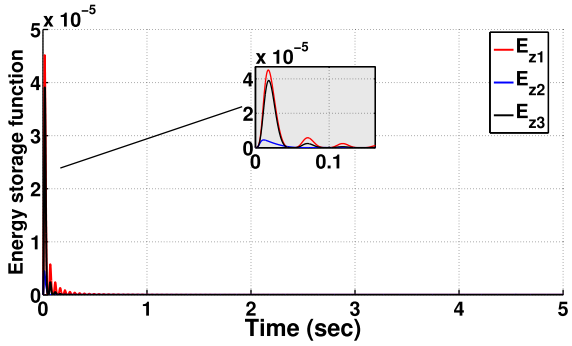

FIGURE 19. Energy storage function about z_m-axis.

function concerning time. According to the illustration, both the total energy and the desired energy converge toward zero as the system approaches its desired angular position. It's worth noting that the energy storage function is a function of the difference between the system's total energy and the desired energy. Hence, obtaining an ideal system response is achievable by using appropriate control strategies embedded within the system's operation.

Fig. 19 illustrates the variation of the energy storage function with respect to time around the Z-axis. During the transient period, the difference between the reference input and the system output is more significant. Therefore, there is a greater difference between the system's total energy and the desired energy during this period. In the steady state, the energy storage function reaches a minimum at the desired position of the magnetic needle.

VI. CONCLUSION

The research findings highlight the significance of the novel 2-D inverted magnetic needle system and its potential applications in control theory. Our study investigates the dynamics of this system, considering both uniform and non-uniform external magnetic fields. This unique system provides opportunities for innovative control approaches based on magnetic needle dynamics, which have practical applications. To stabilize the system and improve its transient and steady-state performance, we design an energy-based controller based on the Lyapunov function. Furthermore, we carried out a thorough examination and comparison of various control techniques' transient and study-state performance with the MPC controller. Our analysis and simulation results show the effectiveness of MPC controller over energy-based control strategies and the optimization of system response through accurate modeling of non-uniform external magnetic fields. This research paves the way for future exploration and experimentation in this field.

Future research can focus on developing advanced control strategies tailored specifically to the dynamics of this system. Nonlinear control methods, adaptive control approaches, and optimal control techniques could be investigated to enhance tracking performance, stability, or energy efficiency. Additionally, addressing the challenge of under-actuation, where there are fewer control inputs than degrees of freedom, presents an important research direction. Finding effective ways to handle under-actuation can lead to practical applications of the inverted magnetic needle system in real-world scenarios.

The authors declare that they have no conflict of interest.

REFERENCES

[1] B. Lu, D. Falde, E. Iriarte, and E. Besnard, "Switching robust control for a nanosatellite launch vehicle," *Aerosp. Sci. Technol.*, vol. 42, pp. 259–266, Apr. 2015.

[2] A. G. Silva and W. C. L. Filho, "Launch vehicle attitude control system using PD plus phase lag," *IFAC Proc. Volumes*, vol. 46, no. 19, pp. 48–53, 2013.

[3] Y. Ma, J. Guo, and S. Tang, "High angle of attack command generation technique and tracking control for agile missiles," *Aerosp. Sci. Technol.*, vol. 45, pp. 324–334, Sep. 2015.

[4] E. Garcia, D. W. Casbeer, and M. Pachter, "Active target defense using first order missile models," *Automatica*, vol. 78, pp. 139–143, Apr. 2017.

[5] H. G. Nguyen, J. Morrell, K. D. Mullens, A. B. Burmeister, S. Miles, N. Farrington, K. M. Thomas, and D. W. Gage, "Segway robotic mobility platform," *Opt. East*, pp. 207–220, Dec. 2004.

[6] G. Pujol and L. Acho, "Stabilization of the Furuta Pendulum with backlash using H_∞-LMI technique: Experimental validation," *Asian J. Control*, vol. 12, no. 4, pp. 460–467, Jul. 2010.

[7] Y. Zheng, X. Li, and L. Xu, "Balance control for the first-order inverted pendulum based on the advantage actor-critic algorithm," *Int. J. Control, Autom. Syst.*, vol. 18, no. 12, pp. 3093–3100, Dec. 2020.

[8] F. Grasser, A. D'Arrigo, S. Colombi, and A. C. Rufer, "JOE: A mobile, inverted pendulum," *IEEE Trans. Ind. Electron.*, vol. 49, no. 1, pp. 107–114, Feb. 2002.

[9] Q. Xu, G. Stepan, and Z. Wang, "Balancing a wheeled inverted pendulum with a single accelerometer in the presence of time delay," *J. Vib. Control*, vol. 23, no. 4, pp. 604–614, Mar. 2017.

[10] C. W. Tao, J. S. Taur, T. W. Hsieh, and C. L. Tsai, "Design of a fuzzy controller with fuzzy swing-up and parallel distributed pole assignment schemes for an inverted pendulum and cart system," *IEEE Trans. Control Syst. Technol.*, vol. 16, no. 6, pp. 1277–1288, Nov. 2008.

[11] D. Chatterjee, A. Patra, and H. K. Joglekar, "Swing-up and stabilization of a cart-pendulum system under restricted cart track length," *Syst. Control Lett.*, vol. 47, no. 4, pp. 355–364, Nov. 2002.

[12] W. Zhong and H. Rock, "Energy and passivity based control of the double inverted pendulum on a cart," in *Proc. IEEE Int. Conf. Control Appl.*, Sep. 2001, pp. 896–901.

[13] M. Deng, A. Inoue, T. Henmi, and N. Ueki, "Analysis and experiment on simultaneous swing-up of a parallel cart-type double inverted pendulum," *Asian J. Control*, vol. 10, no. 1, pp. 121–128, Jan. 2008.

[14] Z. Ben Hazem, M. J. Fotuhi, and Z. Bingül, "A comparative study of the joint neuro-fuzzy friction models for a triple link rotary inverted pendulum," *IEEE Access*, vol. 8, pp. 49066–49078, 2020.

[15] J. E. Marsden and J. Scheurle, "Lagrangian reduction and the double spherical pendulum," *ZAMP Zeitschrift für Angew. Math. und Physik*, vol. 44, no. 1, pp. 17–43, Jan. 1993.

[16] H. Lee and S. Jung, "Balancing and navigation control of a mobile inverted pendulum robot using sensor fusion of low cost sensors," *Mechatronics*, vol. 22, no. 1, pp. 95–105, Feb. 2012.

[17] G. Karam and M. Tabbara, "Rocking blocks stability under critical pulses from near-fault earthquakes using a novel energy based approach," *Appl. Sci.*, vol. 10, no. 17, p. 5924, Aug. 2020.

[18] M. W. Spong, S. Hutchinson, and M. Vidyasagar, *Robot Modeling and Control*, vol. 3. New York, NY, USA: Wiley, 2006.

[19] M. Vidyasagar, *Nonlinear Systems Analysis*. Philadelphia, PA, USA: SIAM, 2002.

[20] J. Drgoňa, J. Arroyo, I. C. Figueroa, D. Blum, K. Arendt, D. Kim, E. P. Ollé, J. Oravec, M. Wetter, D. L. Vrabie, and L. Helsen, "All you need to know about model predictive control for buildings," *Annu. Rev. Control*, vol. 50, pp. 190–232, Jan. 2020.

[21] L. Hewing, K. P. Wabersich, M. Menner, and M. N. Zeilinger, "Learning-based model predictive control: Toward safe learning in control," *Annu. Rev. Control, Robot., Auto. Syst.*, vol. 3, no. 1, pp. 269–296, May 2020.

[22] J. Tarragona, A. L. Pisello, C. Fernández, A. de Gracia, and L. F. Cabeza, "Systematic review on model predictive control strategies applied to active thermal energy storage systems," *Renew. Sustain. Energy Rev.*, vol. 149, Oct. 2021, Art. no. 111385.

[23] R. Liu, J. Wu, and D. Wang, "Sampled-data fuzzy control of two-wheel inverted pendulums based on passivity theory," *Int. J. Control, Autom. Syst.*, vol. 16, no. 5, pp. 2538–2548, Oct. 2018.

[24] V. Utkin, J. Guldner, and J. Shi, *Sliding Mode Control in Electro-Mechanical Systems*, vol. 34. Boca Raton, FL, USA: CRC Press, 2009.

[25] J. Huang, Z.-H. Guan, T. Matsuno, T. Fukuda, and K. Sekiyama, "Sliding-mode velocity control of mobile-wheeled inverted-pendulum systems," *IEEE Trans. Robot.*, vol. 26, no. 4, pp. 750–758, Aug. 2010.

[26] J. Ghabi and H. Dhouibi, "Discrete time sliding mode controller using a disturbance compensator for nonlinear uncertain systems," *Int. J. Control, Autom. Syst.*, vol. 16, no. 3, pp. 1156–1164, Jun. 2018.

[27] D. Zehar, K. Benmahammed, and K. Behih, "Control for underactuated systems using sliding mode observer," *Int. J. Control, Autom. Syst.*, vol. 16, no. 2, pp. 739–748, Apr. 2018.

[28] K. Furuta, M. Yamakita, and S. Kobayashi, "Swing up control of inverted pendulum," in *Proc. Int. Conf. Ind. Electron., Control Instrum. (IECON)*, vol. 91, Oct. 1991, pp. 2193–2198.

[29] N. Muskinja and B. Tovornik, "Swinging up and stabilization of a real inverted pendulum," *IEEE Trans. Ind. Electron.*, vol. 53, no. 2, pp. 631–639, Apr. 2006.

[30] M. Ryalat, D. S. Laila, and H. ElMoaqet, "Adaptive interconnection and damping assignment passivity based control for underactuated mechanical systems," *Int. J. Control, Autom. Syst.*, vol. 19, no. 2, pp. 864–877, Feb. 2021.

[31] B. Yi, R. Ortega, and W. Zhang, "Smooth, time-invariant regulation of nonholonomic systems via energy pumping-and-damping," *Int. J. Robust Nonlinear Control*, vol. 30, no. 16, pp. 6399–6413, Nov. 2020.

[32] X. Huang, Y. Chen, and J. Zhan, "Observer-based consensus control for multi-agent systems with measurement noises and external disturbances," *Int. J. Robust Nonlinear Control*, vol. 32, no. 1, pp. 344–357, Jan. 2022.

[33] S. Hao, Y. Yamashita, and K. Kobayashi, "Robust passivity-based control design for active nonlinear suspension system," *Int. J. Robust Nonlinear Control*, vol. 32, no. 1, pp. 373–392, Jan. 2022.

[34] N. P. Nguyen, H. Oh, Y. Kim, and J. Moon, "A nonlinear hybrid controller for swinging-up and stabilizing the rotary inverted pendulum," *Nonlinear Dyn.*, vol. 104, no. 2, pp. 1117–1137, Apr. 2021.

[35] H. Homburger, S. Wirtensohn, and J. Reuter, "Swinging up and stabilization control of the Furuta Pendulum using model predictive path integral control," in *Proc. 30th Medit. Conf. Control Autom. (MED)*, Jun. 2022, pp. 7–12.

[36] F. F. M. El-Sousy, K. A. Alattas, O. Mofid, S. Mobayen, and A. Fekih, "Robust adaptive super-twisting sliding mode stability control of underactuated rotational inverted pendulum with experimental validation," *IEEE Access*, vol. 10, pp. 100857–100866, 2022.

[37] A. Ma'arif, M. A. M. Vera, M. S. Mahmoud, S. Ladaci, A. Çakan, and J. N. Parada, "Backstepping sliding mode control for inverted pendulum system with disturbance and parameter uncertainty," *J. Robot. Control*, vol. 3, no. 1, pp. 86–92, Nov. 2021.

[38] R. Mondal and J. Dey, "A novel design methodology on cascaded fractional order (FO) PI-PD control and its real time implementation to cart-inverted pendulum system," *ISA Trans.*, vol. 130, pp. 565–581, Nov. 2022.

[39] P. S. Kumar, H. Priyadarshan, and M. H. Simha, "Modeling and implementation of 1-D inverted magnetic needle system using a robust sliding mode controller," *Trans. Inst. Meas. Control*, vol. 42, no. 5, pp. 1037–1046, Mar. 2020.

[40] P. S. Kumar, H. Priyadarshan, and M. S. H. Simha, "Study of robust control performance for inverted magnetic needle," in *Proc. Indian Control Conf. (ICC)*, Jan. 2016, pp. 267–272.

[41] P. S. Kumar, H. Priyadarshan, and M. S. H. Simha, "2-D inverted magnetic needle modeling and it's control: A novel benchmark problem in control system," *IFAC-PapersOnLine*, vol. 49, no. 1, pp. 53–58, 2016.

[42] A. J. Petruska and J. J. Abbott, "Optimal permanent-magnet geometries for dipole field approximation," *IEEE Trans. Magn.*, vol. 49, no. 2, pp. 811–819, Feb. 2013.

[43] K. J. Åström and K. Furuta, "Swinging up a pendulum by energy control," *Automatica*, vol. 36, no. 2, pp. 287–295, Feb. 2000.

[44] G. F. Franklin, J. D. Powell, A. Emami-Naeini, and J. D. Powell, *Feedback Control of Dynamic Systems*, vol. 2. Reading, MA, USA: Addison-Wesley, 1994.

P. SURESH KUMAR received the Ph.D. degree in design of control systems from the Indian Institute of Space Science and Technology (IIST-ISRO) and the master's degree from NIT Trichy. He is currently an Assistant Professor with the Autonomous Vehicles Research Laboratory, Automotive Research Center (ARC), Vellore Institute of Technology (VIT), Vellore. With a strong background in modeling and controller design, he has published extensively in renowned scientific journals and presented his research at international conferences. His expertise lies mainly in autonomous aerial, ground vehicles, and electric vehicles. He actively engages in interdisciplinary collaborations, aiming to bridge the gap between theory and observation. As a Passionate Educator, he inspires students through his engaging teaching methods and encourages their involvement in cutting-edge research projects.

B. ASHOK received the Ph.D. degree from the School of Mechanical Engineering, VIT, Vellore, in 2017. Currently, he is an Associate Professor with the Department of Automotive Technology, School of Mechanical Engineering, VIT. His research interests include automotive engineering, electric and hybrid vehicle powertrain calibration, IC engines, and automotive electronics. His research work is aimed at motor control algorithm development for electric vehicle applications. He has been awarded as top 2 % scientist in the world by a study conducted by researchers with Stanford University.

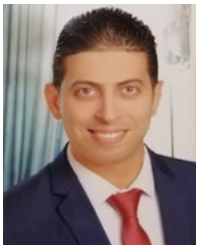

HOSSAM KOTB received the B.Sc., M.Sc., and Ph.D. degrees in electrical engineering from the Faculty of Engineering, Alexandria University, Alexandria, Egypt, in 2009, 2013, and 2020, respectively. His Ph.D. research work is focused on the performance enhancement of renewable energy conversion systems. Currently, he is an Assistant Professor with the Electrical Power and Machines Department, Faculty of Engineering, Alexandria University. His research interests include power system analysis, electrical drives, modern control techniques, smart grids, optimization, electric vehicles, and renewable energy systems. He is also an Associate Editor of *Alexandria Engineering Journal* (AEJ).

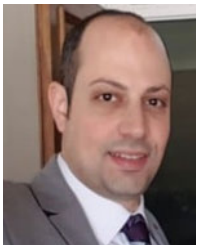

KAREEM M. ABORAS received the B.Sc., M.Sc., and Ph.D. degrees in electrical engineering from the Faculty of Engineering, Alexandria University, Alexandria, Egypt, in 2010, 2015, and 2020, respectively. His Ph.D. research work is focused on the performance enhancement of renewable energy conversion systems. Currently, he is an Assistant Professor with the Electrical Power and Machines Department, Faculty of Engineering, Alexandria University. His research interests include power electronics, control, drives, power systems, and renewable energy systems. He is a reviewer of IET journal.

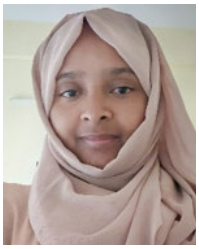

SEADA HUSSEN was born in Wollo, Ethiopia, in 1992. She received the B.Sc. degree in electrical and computer engineering (power stream) from Haramaya University, in 2015, and the M.Sc. degree in power system engineering from Addis Ababa Science and Technology University, in 2020. She is currently pursuing the Ph.D. degree in electrical power engineering with Adama Science and Technology University. She has published 23 research articles in reputed journals and conference publications. She is also with Haramaya University as a Lecturer and a Researcher. She is also serving as an editor and/or a reviewer for different international journals.